Available online at www.sciencedirect.com
ScienceDirect
International Journal of Heat and Mass Transfer 51 (2008) 4717–4727
International Journal of HEAT and MASS TRANSFER
www.elsevier.com/locate/ijhmt

Height and stability of laminar plane fountains in a homogeneous fluid

N. Srinarayana [a,*], G.D. McBain [a], S.W. Armfield [a], W.X. Lin [b]

[a] School of Aerospace, Mechanical and Mechatronic Engineering, The University of Sydney, Sydney, NSW 2006, Australia
[b] School of Engineering, James Cook University, Townsville, Qld 4811, Australia

Received 19 October 2007; received in revised form 24 February 2008
Available online 22 April 2008

Abstract

The behaviour of plane fountains, resulting from the injection of a denser fluid upwards into a large body of a lighter homogeneous fluid, is investigated numerically. The transient behaviour of fountains with a uniform inlet velocity, Reynolds number $Re = 100$, Prandtl number $Pr = 7$, and Froude number $0.25 \leqslant Fr \leqslant 10.0$ is studied numerically. In the present case, the density variation is as a result of temperature difference between the fountain and the ambient fluids. Three distinct regimes are identified; steady and symmetric fountains for $0.25 \leqslant Fr \leqslant 2.0$, unsteady fountains with periodic lateral oscillation for $2.25 \leqslant Fr \leqslant 3.0$, and unsteady fountains with aperiodic lateral oscillations for $Fr \geqslant 4.0$. It is found empirically that the non-dimensional fountain height, z_m, scales differently with Froude number in each of these regimes; in the steady and symmetric region $z_m \sim Fr$, in the unsteady and periodic lateral oscillation region $z_m \sim Fr^{1.15}$ and in the unsteady and aperiodic lateral oscillation region $z_m \sim Fr^{4/3}$. The results are compared with previous numerical and experimental results, where available and are consistent.

Keywords: Plane fountain; Buoyancy dominated flows; Numerical simulation; Scaling; Flapping; Fountain stability

1. Introduction

A fountain forms whenever a fluid is injected upwards into a lighter fluid, or downward into a denser fluid. In the former case the jet penetrates some distance and falls back as a plunging plume around the entering fluid.

Fountains are found in many engineering applications: the heating of a large open structure, such as an aircraft hanger, by large fan-driven heaters at the ceiling level; cooling of turbine blades; cooling of electronic components; the mixing of a two-layer water reservoir with propellers; and the mixing in metallurgical furnaces by gas bubble plumes, to name just a few. Hence, it is important to understand the fundamental physics of such flows.

The behaviour of plane fountains is governed by the Reynolds, densimetric Froude, and Prandtl numbers, defined in the case of a uniform inlet velocity as,

$$Re \equiv \frac{V_{\text{in}} X_{\text{in}}}{\nu},$$
$$Fr \equiv \frac{V_{\text{in}}}{\sqrt{g(\rho_{\text{in}} - \rho_\infty)/\rho_\infty X_{\text{in}}}} = \frac{V_{\text{in}}}{\sqrt{g\beta(T_\infty - T_{\text{in}})X_{\text{in}}}}, \tag{1}$$
$$Pr \equiv \frac{\nu}{\kappa},$$

where X_{in} is the half-width of the inlet jet. The second expression of the Froude number applies when the density difference is due to the difference in temperature of the fountain and the ambient fluids using the Oberbeck–Boussinesq approximation. It should also be noted that alternatively Richardson number, $Ri = 1/Fr^2$, has been used in the literature [1–3].

For fountains with a relatively large discharge momentum compared to negative buoyancy flux ($Fr \gg 1$) and a

* Corresponding author. Tel.: +61 2 9351 7140; fax: +61 2 9351 7060.
E-mail address: snag3258@usyd.edu.au (N. Srinarayana).

0017-9310/$ - see front matter © 2008 Elsevier Ltd. All rights reserved.
doi:10.1016/j.ijheatmasstransfer.2008.02.022

Nomenclature

C	constant of proportionality, defined in (2)
D_H	hydraulic diameter
Fr	densimetric Froude number
f	non-dimensional flapping frequency
g	acceleration due to gravity
P	pressure
p	non-dimensional pressure
Pr	Prandtl number
Re	Reynolds number
Ri	Richardson number
T	temperature
U	horizontal velocity
u	non-dimensional horizontal velocity
V	vertical velocity
v	non-dimensional vertical velocity
X	horizontal coordinate
x	non-dimensional horizontal coordinate
Y	vertical coordinate
y	non-dimensional vertical coordinate
z_m	non-dimensional fountain height

Greek symbols

β	coefficient of volumetric expansion
κ	thermal diffusivity
ν	kinematic viscosity
ρ	fluid density
τ	non-dimensional time
θ	non-dimensional temperature

Subscripts

in	variable index at the source
∞	variable index of the ambient

large Reynolds number, the flow becomes turbulent close to the source. Turner [4] in his experiments observed that the velocity decreased with height and the whole fountain broadened, came to rest and fell back, until it settled down to a nearly steady state, with the top at a lower height than that attained by the first pulse, an upflow in the centre and a downflow surrounding the upflow. There was exchange of fluid between the up and the down currents, and the mixing of the upflow with descending fluid rather than the stationary environment accounted for the smaller fountain height in the steady state. The experiments revealed that the fountain height of a turbulent fountain does not remain constant, but oscillates with time.

Baines et al. [5] obtained an analytical scaling:

$$z_m = CFr^{4/3}, \tag{2}$$

for a plane turbulent fountain, if the source size is small compared with the height of the resulting fountain. Baines et al. [5] conducted a series of experiments on plane fountains and found that $C = 0.65$. However, Campbell and Turner [6] obtained $C = 1.64$–1.97 from their experiments on plane turbulent fountains. Zhang and Baddour [7] studied the effect of mass flux, momentum flux and buoyancy flux on the properties of plane turbulent fountains experimentally by using two different models. The first model (virtual source model) applied the concept of virtual origin proposed by Morton [8] and the second model (zero-entrainment model) ignored the turbulent entrainment. For $Fr < 6.5$, their virtual source model gave,

$$z_m = (2.0 - 1.12Fr^{-2/3})Fr^{4/3}, \tag{3}$$

and their zero-entrainment model gave,

$$z_m = 0.71Fr^2. \tag{4}$$

They used scaling equation (2) for large Froude number experiments ($Fr \geqslant 10$) and obtained $C = 2.0$.

Goldman and Jaluria [9] carried out an experimental investigation on plane turbulent fountains by blowing hot air vertically downward into a chamber and obtained $z_m = 5.83Fr^{0.88}$, by regression analysis. Recently, Lin and Armfield [10] investigated the effect of the Reynolds number on the height of plane fountains. They found that for $Re \leqslant 200$ the fountain height was dependent on the Reynolds number with the following scaling:

$$z_m \sim FrRe^{-1/2}. \tag{5}$$

Their numerical investigations [11] demonstrate that for $0.2 \leqslant Fr \leqslant 1.0$, $Re = 200$ and $Pr = 7$ the following relation can be obtained:

$$z_m = 0.2774 + 1.8696Fr. \tag{6}$$

A number of investigations have also been undertaken into axisymmetric (round) fountains. Campbell and Turner [6] gave,

$$z_m = CFr, \tag{7}$$

and obtained $C = 2.46$ [6] from their experiments on turbulent fountains. Turner [4] also found the height of the starting fountain, i.e., the height maximum attained at start-up, to be a factor of 1.43 greater than the steady value [4]. Morton [8] used entrainment equations to quantify the increasing radius, the decreasing buoyancy and the velocity of dense fluid injected upward into a lighter fluid, and obtained $C = 2.05$ analytically. Morton, however, did not consider the effect of the downflow and hence his analysis is only valid before the fountain falls back. Abraham [12] proposed an analytical solution in which he considered the decrease of the vertical flux of a tracer near the top of the fountain, which was not present in the previous study by Morton [8], where a constant vertical flux was assumed, obtaining $C = 2.74$. Mizushina et al. [13], experimentally investigated a jet discharged upwards into an

ambient of higher temperature than that of the jet fluid and obtained $C = 2.35$. An experimental investigation was conducted by Zhang and Baddour [14] to study the effect of source mass flux on the maximum penetration of a vertical dense jet. Their experiments mainly focused on small Froude number jets where the source mass flux cannot be neglected and showed that mass flux had no effect on maximum height at large Froude numbers ($Fr > 7.0$), but reduced the height at small Froude numbers ($Fr > 7.0$).

Lin and Armfield [10] obtained $z_m \sim Fr$, analytically, which was validated by a range of numerical simulations with $0.1 \leqslant Fr \leqslant 1.0$, $Re = 200$ and $Pr = 7$ [15]. Recently, there have been many experimental studies on fountains notably by Friedman and Katz [1], Philippe et al. [16] and Kaye and Hunt [17], quantifying z_m in terms of source Fr and Friedman [2] and Friedman et al. [3] studied the oscillations in height and instability thresholds of fountains. As shown above similar scaling relations have been obtained by various researchers, however there are significant variations in the constant of proportionality [18]. Details of other numerical and experimental investigations on fountains and buoyancy dominated flows, apart from the works mentioned above, can be found in [19–32].

In this study, we investigate the influence of the Froude number on plane fountains and obtain empirical relations between the height and the Froude number for $Re = 100$, $0.25 \leqslant Fr \leqslant 10.0$ and $Pr = 7$. Additionally, we obtain the critical Froude number for a flapping instability. The current work is a direct extension of the weak fountains ($Fr \leqslant 1.0$) investigations of Lin and Armfield [10,11]. Lin and Armfield assumed the flow to be symmetric about the fountain source, and used a boundary condition configuration that limited the total integration time. In the present investigation the viscosities of the fluids are fixed.

The outline of the paper is as follows. In Section 2 we describe the computational domain and numerical scheme. In Section 3, the results are presented followed by discussions in Section 4. Finally, the paper is summarised in Section 5.

2. Numerical model

The fluid between horizontal insulated solid walls a distance H apart is initially still and isothermal at temperature T_∞. For $t \geqslant 0$ fluid issues from a slot of width $2X_{\text{in}}$ in the floor with a uniform velocity V_{in} and temperature $T_{\text{in}} < T_\infty$. The flow is assumed to remain two-dimensional. Fig. 1 shows the computational domain. The buoyancy is a result of the temperature difference between the source and the ambient fluids.

The governing equations are the incompressible Navier–Stokes equations with the Oberbeck–Boussinesq approximation. The following equations are written in conservative, non-dimensional form in Cartesian coordinates,

$$\frac{\partial u}{\partial x} + \frac{\partial v}{\partial y} = 0, \tag{8}$$

$$\frac{\partial u}{\partial \tau} + \frac{\partial (uu)}{\partial x} + \frac{\partial (vu)}{\partial y} = -\frac{\partial p}{\partial x} + \frac{1}{Re}\left(\frac{\partial^2 u}{\partial x^2} + \frac{\partial^2 u}{\partial y^2}\right), \tag{9}$$

$$\frac{\partial v}{\partial \tau} + \frac{\partial (uv)}{\partial x} + \frac{\partial (vv)}{\partial y} = -\frac{\partial p}{\partial y} + \frac{1}{Re}\left(\frac{\partial^2 v}{\partial x^2} + \frac{\partial^2 v}{\partial y^2}\right) + \frac{1}{Fr^2}\theta, \tag{10}$$

$$\frac{\partial \theta}{\partial \tau} + \frac{\partial (u\theta)}{\partial x} + \frac{\partial (v\theta)}{\partial y} = \frac{1}{RePr}\left(\frac{\partial^2 \theta}{\partial x^2} + \frac{\partial^2 \theta}{\partial y^2}\right). \tag{11}$$

The following non-dimensionalisation is used:

$$x = \frac{X}{X_{\text{in}}}, \quad y = \frac{Y}{X_{\text{in}}}, \quad u = \frac{U}{V_{\text{in}}}, \quad v = \frac{V}{V_{\text{in}}},$$
$$\tau = \frac{t}{(X_{\text{in}}/V_{\text{in}})}, \quad p = \frac{P}{\rho V_{\text{in}}^2}, \quad \theta = \frac{T - T_\infty}{T_\infty - T_{\text{in}}}. \tag{12}$$

The initial and boundary conditions are,

$$u = v = \theta = 0 \text{ when } \tau < 0, \tag{13}$$

and when $\tau \geqslant 0$,

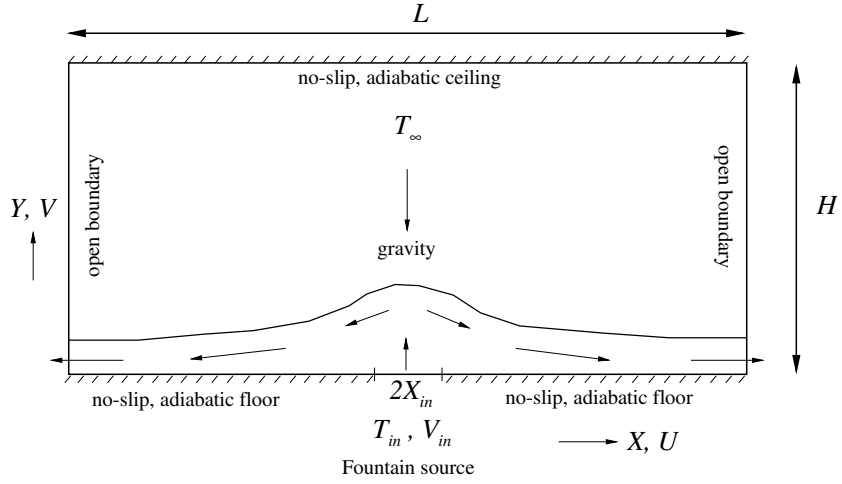

Fig. 1. Computational domain.

Open boundaries at left and right edges:

$$\frac{\partial u}{\partial x}=0,\quad \frac{\partial v}{\partial x}=0,\quad \frac{\partial \theta}{\partial x}=\ 0 \text{ on } x=\pm L/(2X_{\text{in}}), \tag{14}$$

isothermal uniform velocity at inlet:

$$u=0,\quad v=1,\quad \theta=-1 \text{ on } |x|\leqslant 1,\quad y=0, \tag{15}$$

no-slip adiabatic floor:

$$u=v=0,\quad \frac{\partial \theta}{\partial y}=0 \text{ on } |x|>1,\quad y=0, \tag{16}$$

no-slip adiabatic ceiling:

$$u=v=0,\quad \frac{\partial \theta}{\partial y}=0 \text{ on } y=H/X_{\text{in}}, \tag{17}$$

respectively. The open boundaries at the left and right edges are based on the assumption that the variation of flow variables in the boundary normal direction is negligible. Additionally, it is ensured that the open boundaries are sufficiently far from the region of interest.

The results were obtained using the open source code Gerris [33], a quad-tree based adaptive mesh solver which uses a fractional-step projection method. The advective terms are discretised using a second-order Godunov type scheme, the remaining terms use standard second-order schemes and the equations are solved using a semi-implicit multi-grid approach. The computational domain is $-100\leqslant x\leqslant +100$ and $0\leqslant y\leqslant 100$. The minimum grid spacing is 4.88×10^{-4} in each direction. The mesh is dynamically adapted based on the vorticity and the temperature. The adaptive refinement is performed at the fractional time-step. A cell is refined, i.e. divided into four square sub-cells, whenever

$$\frac{|\nabla\times v|\Delta x}{\max|v|}>\delta,\quad |\nabla\theta|\Delta x>\delta, \tag{18}$$

where Δx is the size of the cell and δ is a user-defined threshold which can be interpreted as the maximum angular deviation (caused by the local vorticity) of a particle travelling at a speed $\max|v|$ across the cell. The cells are also coarsened likewise. The code has been tested for different values of δ and CFL numbers, more specifically δ was halved each time and was tested for 0.04, 0.02, 0.01 and 0.005 and CFL number was tested for 1.0, 0.75, 0.5 and 0.25. The variation in fountain height from $\delta=0.01$ to $\delta=0.005$ and from CFL = 0.5 to CFL = 0.25 was found to be less than 1%, and $\delta=0.01$ and CFL = 0.5 have been used throughout in the numerical calculations. The time-step varies dynamically during the iteration process, to maintain a constant CFL. As an example at full development a time-step of 2.15×10^{-4} resulted for $Fr=2.0$. The number of cells also varies with Fr due to the adaptive nature of the algorithm. A typical mesh, for $Fr=2.0$, is shown in Fig. 2, with 114750 cells. Runs times are of the order of 27 h on a typical 3.2 GHz Pentium-IV machine with 1GB RAM.

3. Results

An overview of the temperature fields at different times for $Fr=2.0$ and $Fr=2.25$ is shown in Fig. 3. After the fountain is initiated, it travels upwards until momentum balances buoyancy, when it comes to rest. The rising fluid spreads due to its reduced velocity and interaction with the ambient fluid. The descending fluid then interacts with the environment and with the upflow, restricting the rise of fur-

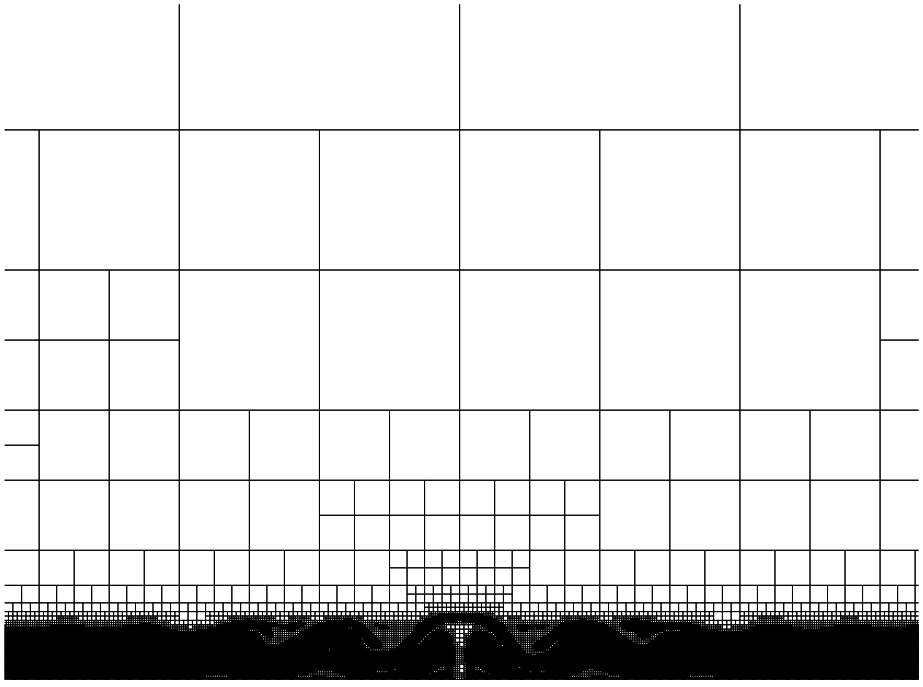

Fig. 2. A typical adapted mesh.

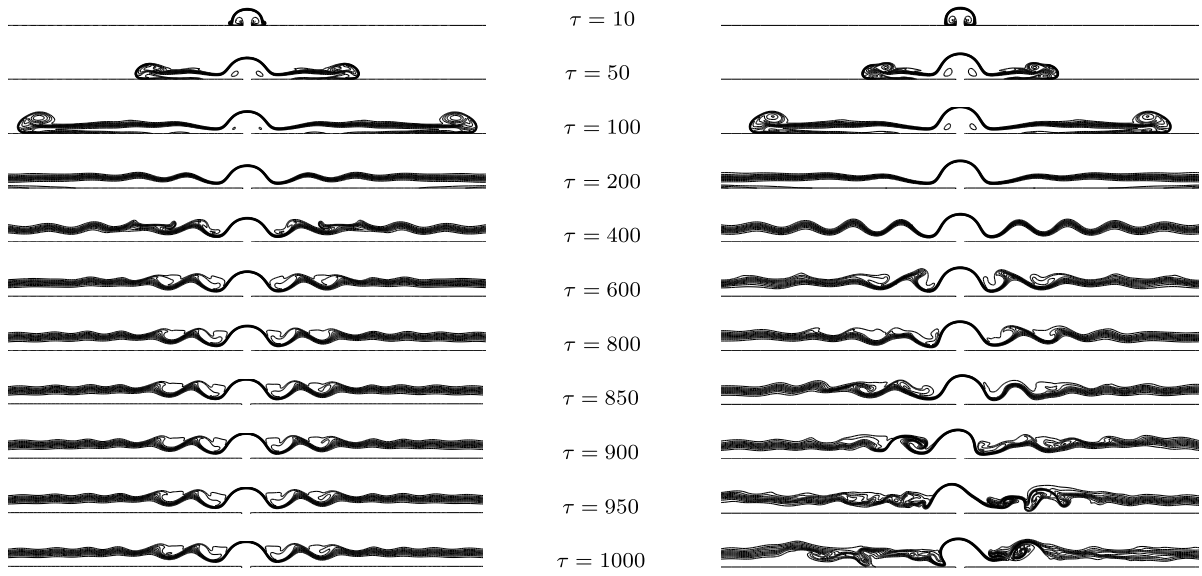

Fig. 3. Evolution of temperature fields for $Fr = 2.0$ (left column) and $Fr = 2.25$ (right column).

ther fluid. The descending fluid, heavier than the ambient, moves along the floor as a gravity current. Once full development is reached, the fountain is symmetric and steady for $Fr = 2.0$. The fountain starts symmetrically for $Fr = 2.25$ and the initial fountain structure is similar to that of $Fr = 2.0$ except that in case of $Fr = 2.25$ the fountain has

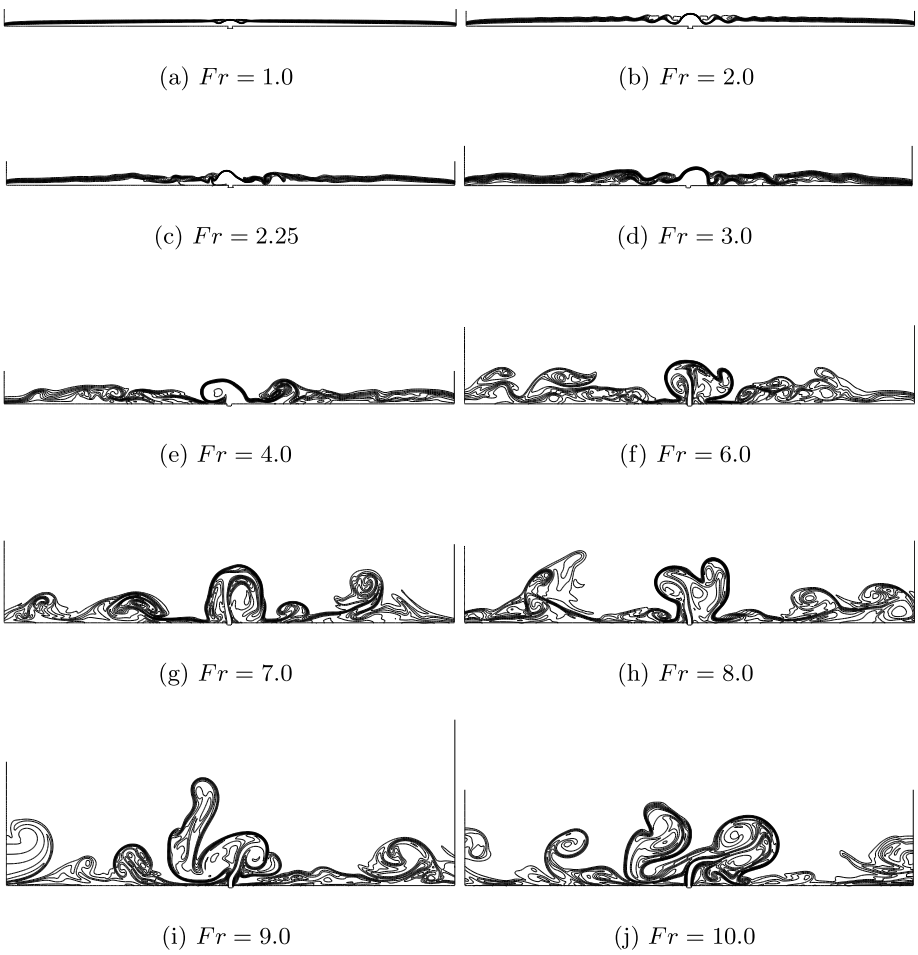

Fig. 4. Instantaneous temperature fields after the flow is fully developed.

a shorter intrusion length for the same non-dimensional time. This is due to the reduced buoyancy force at higher Fr. Eventually, the fountain for $Fr = 2.25$ becomes asymmetric. Observations of animations for this flow show that the asymmetry is associated with an unsteady flow, whereby the fountain flaps from side to side. This flapping motion is associated with repeated shedding of the top section of the fountain to the side, exposing the core which then increases in height and shifts to the other side. For $Fr = 2.25$ this flapping motion is periodic, while for higher Fr, it is aperiodic, as discussed below.

Fig. 4 shows the instantaneous temperature fields at full development for different Froude numbers. The fountains are observed to be symmetric for $Fr \leqslant 2.0$, but asymmetric for the higher Froude numbers ($Fr \geqslant 2.25$). In all cases the asymmetry is associated with unsteady flow in the form of a periodic or quasi-periodic flapping motion, as described above, for $Fr = 2.25$ and 3.0, and a more unstructured and chaotic motion for $Fr \leqslant 4.0$. A general increase in fountain height with Fr can also be observed in these results. The chaotic behaviour of the higher Froude number flow is demonstrated in Fig. 5, where the time-evolution of a typical high Froude number ($Fr = 8.0$) fountain is shown. The starting structure shows a flow similar to a starting jet, with the typical double vortex head entraining ambient fluid that forms the initial downflow region on either side of the fountain core. The start-up flow reaches an initial maximum height, shown in Fig. 5d, with the subsequent reduction in height resulting from the interaction of the core with the downflow fluid. The fountain becomes asymmetric at this time, and a strong unsteady chaotic motion is observed in the subsequent development of the flow. At this Froude number the fountain undergoes an aperiodic flapping motion, and this, together with associated shedding of the fountain top, is seen at the subsequent times shown in Fig. 5.

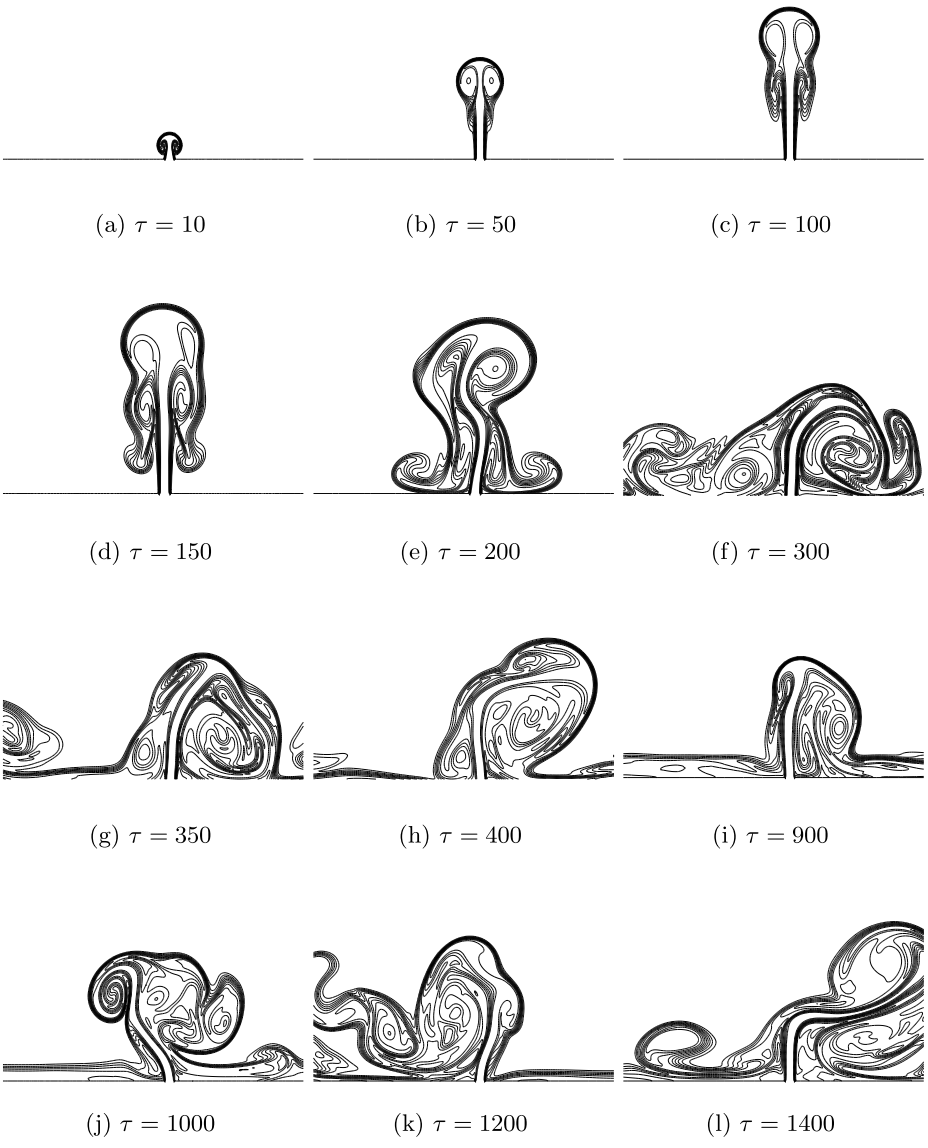

Fig. 5. Evolution of temperature fields for $Fr = 8.0$.

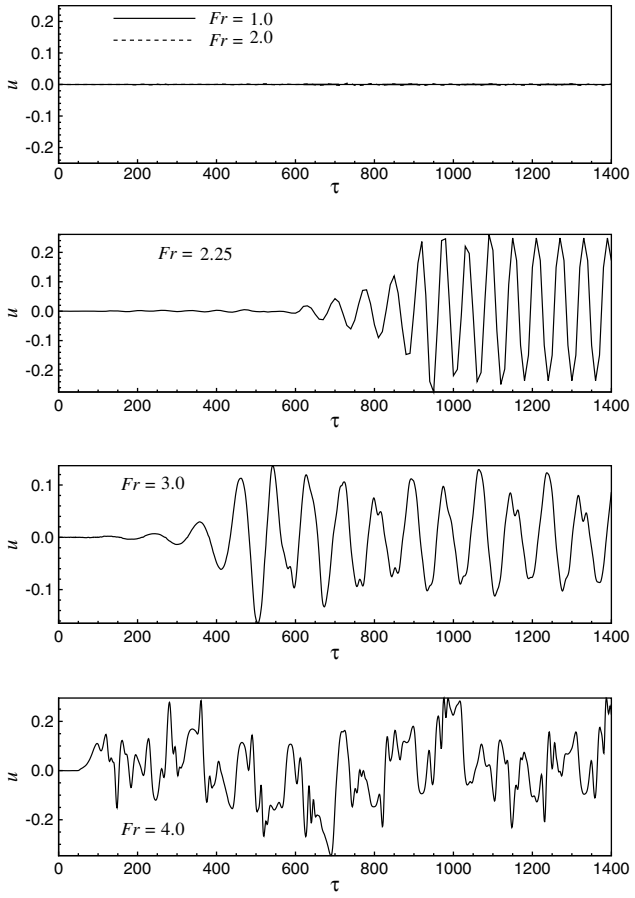

Fig. 6. Time series of u at $x = 0$ and $y = 2$ for different Froude numbers.

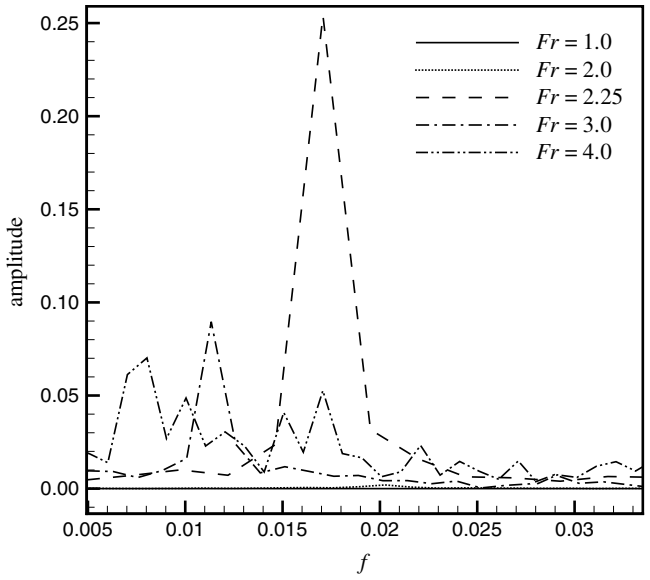

Fig. 7. Frequency spectrum of u for different Froude numbers.

This variation in fountain behaviour with Froude number is examined further in Fig. 6 which shows the time-evolution of u at $x = 0$ and $y = 2$. The horizontal velocity is almost zero for $Fr = 1.0$ and 2.0, indicating that the fountain is symmetric about $x = 0$ and steady. For $Fr = 2.25$, the flow is seen to transition from an initially steady, symmetric, state to an unsteady state, with a periodic signal. Similar behaviour is seen for $Fr = 2.5$ and 2.75 (not shown here) and a quasi-periodic signal observed for $Fr = 3.0$ and an aperiodic, chaotic signal observed for $Fr = 4.0$. This behaviour is further demonstrated in Fig. 7 which contains the non-dimensional frequency spectrum f, inverse of non-dimensional period of oscillation $= 1/\Delta\tau$, where $\Delta\tau$ is the distance between successive peak of oscillation, of the signals given above in Fig. 6, obtained using discrete Fourier transforms. The change in flow behaviour between $Fr = 2.0$ and 2.25 is again clearly seen, with a negligible spectral amplitude at $Fr = 2.0$, and a strong single mode signal at $Fr = 2.25$, with $f \sim 0.017$, demonstrating the periodic nature of the flow. Similar single mode behaviour is observed for $Fr = 2.5$ and $Fr = 2.75$ (not shown here), with $f = 0.015$ and $f = 0.013$, respectively. For $Fr = 3.0$ the flow shows a less dominant mode, with $f = 0.011$, with additional smaller higher and lower frequency modes, demonstrating quasi-periodic behaviour. $Fr = 4.0$ shows a broad-banded, multi-modal structure, reflecting the aperiodic chaotic motion observed for higher Froude numbers. Time series obtained at other y-locations for $x = 0$ were found to have identical frequencies as a result of the homogeneous structure of the flapping motion for these Froude numbers.

Fig. 8 shows time series of v at $x = 0$ and $y = 2$. As noted above for the horizontal velocity, v is approximately steady for $Fr = 1.0$ and 2.0. At $Fr = 2.25$, 2.5 and 3.0 the fully developed time series shows unsteady periodic and quasi-periodic signals, while for $Fr = 4.0$ the fully developed flow shows aperiodic, chaotic signals, again as observed for the horizontal velocity at the same location. The frequency spectra for the v signals, obtained using Fourier Transforms, are shown in Fig. 9 for the indicative Froude numbers 1.0, 2.0, 2.25, 3.0 and 4.0. Dominant modes are observed for $Fr = 2.25$ and 3.0, with additional higher and lower modes for $Fr = 3.0$. $Fr = 4.0$ again shows a broad-banded, multi-modal structure. However the frequencies are now $f = 0.033$, 0.030, 0.026 and 0.022 for the dominant modes for $Fr = 2.25$, 2.5, 2.75 and 3.0, almost twice the frequencies obtained for u, given above. This is a result of the structure of the flapping motion at these Froude numbers. The flapping is combined with a bobbing motion, whereby the fountain height is greatest at the left and the right extremities of the flapping, and smallest at the centre. The fountain height thus passes through two maximum heights and two minimum heights for each full cycle of side to side flapping, and this is reflected in the vertical velocity time series, with the observed doubling of the frequency when compared to that of the horizontal velocity, which reflects the side to side motion only.

The fountain height is determined as the y location at which the vertical velocity first goes to zero on the centreline, $x = 0.0$. The variation of the fully developed vertical velocity with y is shown in Fig. 10. For the flows that are

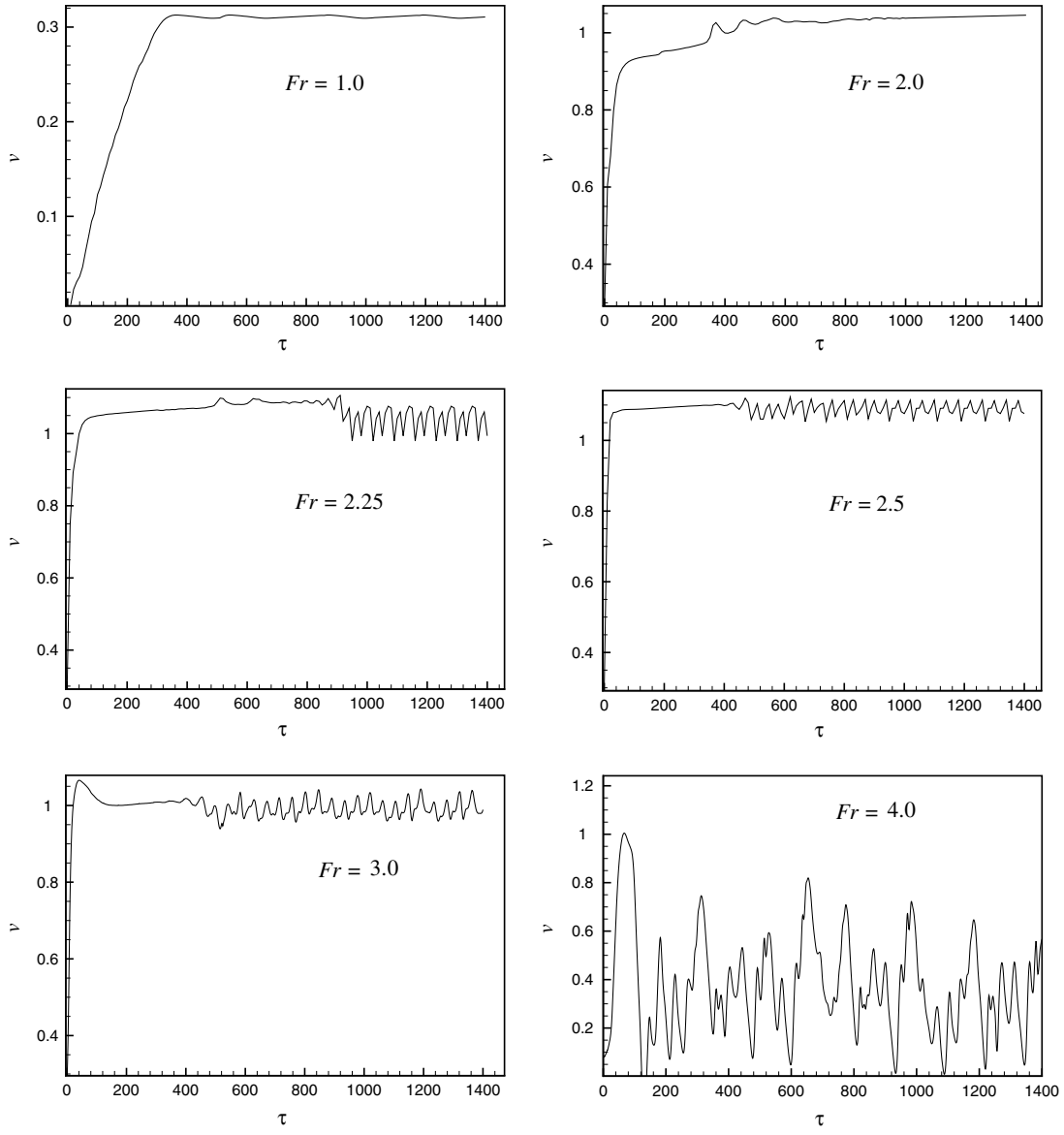

Fig. 8. Time series of v at $x = 0$ and $y = 2$ for different Froude numbers.

unsteady at full development, that is those with $Fr \geqslant 2.25$, the profile shown is obtained by time-averaging over the period $\tau = 400$–1400. The non-dimensional velocity at the source is 1.0. The velocity then decreases with increasing y due to a decrease in the momentum flux, eventually reducing to zero and becoming negative. This negative flow, above the fountain, reflects the entrainment of lighter, ambient fluid by the heavier fountain fluid. Further away from the entrainment region and close to the ceiling (not shown in Fig. 10), the velocity returns to zero.

The variation of time-averaged non-dimensional fountain height with Fr is shown in Fig. 11, with, as noted above, the time-averaging carried out for the period $\tau = 400$–1400. It is observed that the fountain heights may be considered as three distinct groups, each displaying a different behaviour. For the lower Fr values considered, that is $0.25 \leqslant Fr \leqslant 2.0$, the height increases smoothly with Froude number, forming the first group. There is then a discontinuous jump in height from $Fr = 2.0$ to $Fr = 2.25$, followed by the second grouping in which the height increases smoothly again with Froude number, for $2.25 \leqslant Fr \leqslant 3.0$. The third grouping, with Froude numbers $4.0 \leqslant Fr \leqslant 10.0$, shows some scatter, with a non-smooth increase in height with Froude number. These three groupings correspond to the three behaviours observed in the temperature contours, shown in Fig. 4, and in the time series and frequency spectra shown in Figs. 6–9. It is of interest to determine if the variation of fountain height can be represented by simple scaling relations of the type discussed in Section 1, with the observed groupings described above suggesting that three separate scalings may be necessary to obtain a satisfactory fit.

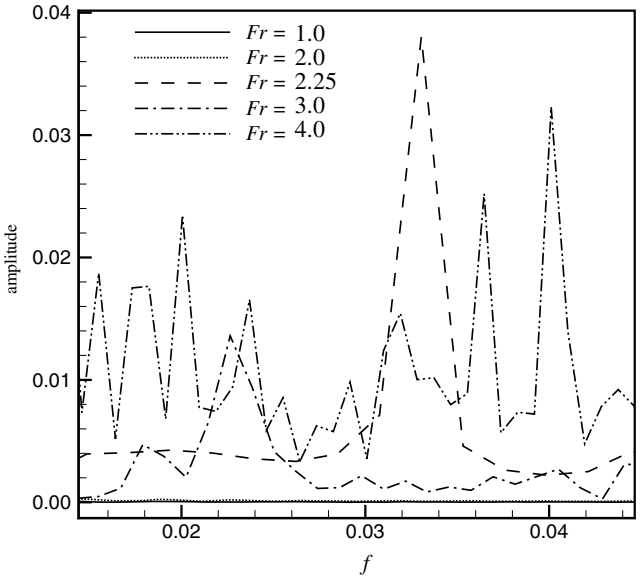

Fig. 9. Frequency spectrum of v for different Froude numbers.

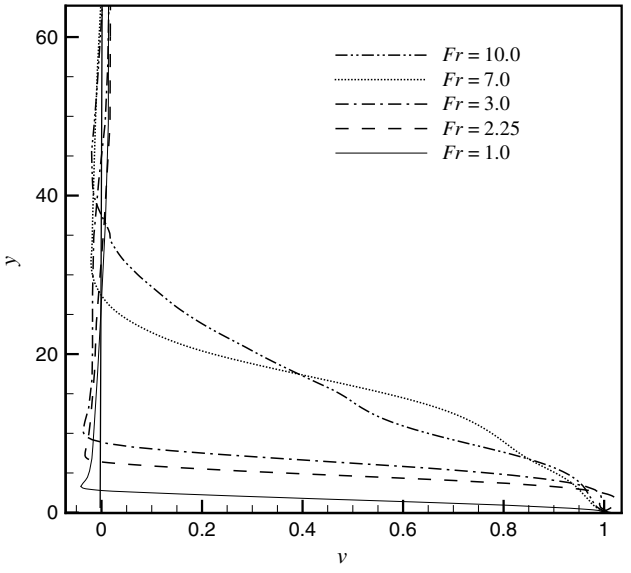

Fig. 10. Profiles of the time-averaged vertical velocity on the centreline for different Fr.

The linear Froude number scaling suggested by Lin and Armfield [10,11] for weak fountains was tested for the first grouping, with regression analysis providing:

$$z_m \equiv 0.64 + 2.22Fr, \tag{19}$$

with a maximum variation of ±0.026. This relation is plotted for the first grouping in Fig. 11 and is seen to provide a good fit.

In the second grouping, consisting of those flows that exhibited periodic and quasi-periodic flapping, the linear Froude number scaling was found to perform poorly. A best fit power law, obtained by regression, was found to be

$$z_m \equiv 2.52Fr^{1.15}, \tag{20}$$

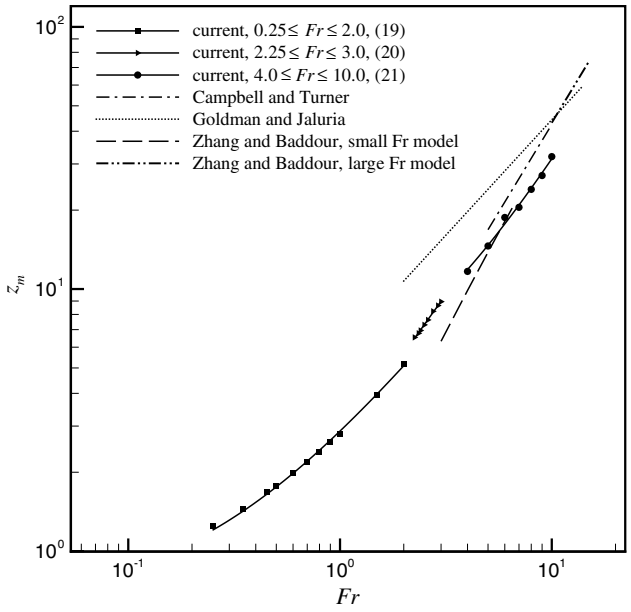

Fig. 11. Variation of fountain height with Froude number.

with a maximum variation of ±0.058. This relation is plotted in Fig. 11 for the second grouping and seen to provide a good fit.

For the high Froude number grouping, representing the aperiodic, chaotic flows, neither the linear scaling, nor the $Fr^{1.15}$ scaling provided a good fit. The $Fr^{4/3}$ scaling, as previously suggested by a number of workers and discussed in Section 1 was tested, with regression analysis giving the relation:

$$z_m \equiv 3.72 + 1.285Fr^{4/3}, \tag{21}$$

with a maximum variation of ±0.32. This relation is plotted in Fig. 11 for the third, high Froude number, grouping, together with the scaling of Campbell and Turner [6], Eq. (2) with C set to 1.75, the scaling of Goldman and Jaluria [9], $z_m = 5.83Fr^{0.88}$, the small Fr virtual source scaling of Zhang and Baddour [7], Eq. (3) and the large Fr scaling of Zhang and Baddour, Eq. (2) with C set to 2.0.

4. Discussions

The transition from a steady and symmetric fountain to an unsteady and asymmetric case occurs between $Fr = 2.0$ and 2.25. This result correlates well with the critical Richardson number obtained in Friedman et al. [3] for the onset of instability in fountains, when the Froude number is expressed in terms of the hydraulic diameter, D_H, rather than the slot half-width for non-circular fountains (for an infinitely long slot $D_H = 4X_{in}$). Adjusting for the choice of length scale, the transition Richardson number (based on D_H) in the present study is $Ri = 1.0$ ($Fr = 2.0$), consistent with $Ri \sim 1.0$ of Friedman et al. [3].

From the present study, the authors note that the frequency of the flapping for the periodic and quasi-periodic

flow regime was observed to reduce with increasing Froude number and, hence, to reduce with increasing fountain height. This is analogous to a pendulum, in which the pendulum period increases with the length of the pendulum. Also, it is noted that the unsteady fountain behaviour is strongly dependent on the fountain entrance geometry. In this case, we have used a fountain entrance that is flush with the bottom of the domain. Alternatively a re-entrant nozzle may be used, and preliminary tests have shown that this will significantly affect the transition behaviour.

The linear Fr scaling of Lin and Armfield [10,11] provided a good fit for $0.25 \leqslant Fr \leqslant 2.0$. However, the variation in the constants obtained with the present data (Eq. (19)) and those of Lin and Armfield (Eq. (6)) is a result of the use of different domain configuration, as mentioned earlier in Section 1. It is observed that the $Fr^{4/3}$ scaling provides a good fit to the numerical data for $4.0 \leqslant Fr \leqslant 10.0$. The numerical data obtained here compares reasonably well with the scaling given by Campbell and Turner [6] and the virtual source model of Zhang and Baddour [7]. The Goldman and Jaluria [9] scaling is seen to produce significantly different results, which may be due to the use of a different method to determine the fountain height, or due to the geometry of their experimental rig. The constant of proportionality ($C = 1.285$) in the Eq. (21) is slightly outside the range given by Campbell and Turner [6].

Some preliminary numerical runs were carried out to determine the Pr dependence of the fountain behaviour for $7 \leqslant Pr \leqslant 700$. The results show negligible variation in the behaviour of the fountain.

5. Conclusions

The long-term transient behaviour of plane fountains with uniform inlet velocity has been studied numerically with $Re = 100$, $0.25 \leqslant Fr \leqslant 10.0$ and $Pr = 7$ using an adaptive mesh solver. Three distinct regimes have been identified. In the first regime, the fountain is symmetric and steady with $0.25 \leqslant Fr \leqslant 2.0$. Similar flow patterns were observed by Lin and Armfield [11] with weak laminar plane fountains ($0.2 \leqslant Fr \leqslant 1.0$). In the second regime ($2.25 \leqslant Fr \leqslant 3.0$), the fountain is unsteady and asymmetric, exhibiting a periodic side to side flapping motion combined with bobbing in which the maximum fountain height is reached twice in each flapping period when the fountain is at the extremity of the flap. In the third regime ($Fr \geqslant 4.0$), the fountain is unsteady and aperiodic. The critical Froude number for transition from steady to unsteady flow therefore lies between $Fr = 2.0$ and 2.25. The transition from steady to unsteady behaviour, with associated critical Froude numbers, are consistent with the experimental results of Friedman et al. [3].

A number of scaling relations have been derived previously relating the fountain height to the Froude number, as detailed in the Introduction. In the low Froude number, steady, symmetric flow regime the linear scaling derived by Lin and Armfield [11] was found to provide a good fit to the numerical data, although as noted above the scaling constants varied from those of Lin and Armfield as a result of the use of different boundary conditions and integration times. In the high Froude number, unsteady and aperiodic regime ($Fr \geqslant 4.0$), the $z_m \sim Fr^{4/3}$ scaling, suggested originally by Baines et. al. [5], was found to provide a good fit. The linear and $Fr^{4/3}$ power scalings were found to provide a poor fit to the numerical data in the periodic and quasi-periodic flapping regime, ($2.25 \leqslant Fr \leqslant 3.0$). For this regime the best fit was found to be of the form $z_m \sim Fr^{1.15}$, obtained by regression, which is seen to lie between the linear low Froude number relation that is suitable for steady flow, and the $Fr^{4/3}$ high Froude number relation, that is suitable for the strongly unsteady, chaotic flow.

Acknowledgement

The support of the Australian Research Council is gratefully acknowledged.

References

[1] P.D. Friedman, J. Katz, Rise height for negatively buoyant fountains and depth of penetration for negatively buoyant jets impinging an interface, ASME J. Fluid Eng. 122 (2000) 779–782.
[2] P.D. Friedman, Oscillation in height of a negatively buoyant jet, J. Fluid Eng. 128 (2006) 880–882.
[3] P.D. Friedman, V.D. Vadakoot, W.J. Meyer Jr., S. Carey, Instability threshold of a negatively buoyant fountain, Exp. Fluid 42 (2007) 751–759.
[4] J.S. Turner, Jets and plumes with negative or reversing buoyancy, J. Fluid Mech. 26 (1966) 779–792.
[5] W.D. Baines, J.S. Turner, I.H. Campbell, Turbulent fountains in an open chamber, J. Fluid Mech. 212 (1990) 557–592.
[6] I.H. Campbell, J.S. Turner, Fountains in magma chambers, J. Petrol. 30 (1989) 885–923.
[7] H. Zhang, R.E. Baddour, Maximum vertical penetration of plane turbulent negatively buoyant jets, J. Eng. Mech. 123 (1997) 973–977.
[8] B.R. Morton, Forced plumes, J. Fluid Mech. 5 (1959) 151–163.
[9] D. Goldman, Y. Jaluria, Effect of opposing buoyancy on the flow in free and wall jets, J. Fluid Mech. 166 (1986) 41–56.
[10] W. Lin, S.W. Armfield, The Reynolds and Prandtl number dependence of weak fountains, Comput. Mech. 31 (2003) 379–389.
[11] W. Lin, S.W. Armfield, Direct simulation of weak laminar plane fountains in a homogeneous fluid, Int. J. Heat Mass Transfer 43 (2000) 3013–3026.
[12] G. Abraham, Jets with negative buoyancy in homogeneous fluid, J. Hydraul. Res. 5 (1967) 235–248.
[13] T. Mizushina, F. Ogino, H. Takeuchi, H. Ikawa, An experimental study of vertical turbulent jet with negative buoyancy, Wärme- und Stoffü bertragung 16 (1982) 15–21.
[14] H. Zhang, R.E. Baddour, Maximum penetration of vertical round dense jets at small and large Froude numbers, J. Hydraul. Eng. 124 (1998) 550–553.
[15] W. Lin, S.W. Armfield, Direct simulation of weak axisymmetric fountains in a homogeneous fluid, J. Fluid Mech. 403 (2000) 67–88.
[16] P. Philippe, C. Raufaste, P. Kurowski, P. Petitjeans, Penetration of a negatively buoyant jet in a miscible liquid, Phys. Fluid 17 (2005). Art. No. 053601.
[17] N.B. Kaye, G.R. Hunt, Weak fountains, J. Fluid Mech. 558 (2006) 319–328.

[18] E.J. List, Turbulent jets and plumes, Ann. Rev. Fluid Mech. 14 (1982) 189–212.
[19] I.H. Campbell, J.S. Turner, Turbulent mixing between fluids with different viscosities, Nature 313 (1985) 39–42.
[20] I.H. Campbell, J.S. Turner, The influence of viscosity on fountains in magma chambers, J. Petrol. 27 (1986) 1–30.
[21] R.A. Seban, M.M. Behnia, K.E. Abreau, Temperature in a heated air jet discharged downward, Int. J. Heat Mass Transfer 21 (1978) 1453–1458.
[22] L.J. Bloomfield, R.C. Kerr, Turbulent fountains in a stratified fluid, J. Fluid Mech. 358 (1998) 335–356.
[23] L.J. Bloomfield, R.C. Kerr, Turbulent fountains in a confined stratified environment, J. Fluid Mech. 389 (1999) 27–54.
[24] L.J. Bloomfield, R.C. Kerr, A theoretical model of a turbulent fountain, J. Fluid Mech. 424 (2000) 197–216.
[25] R.A. Seban, M.M. Behnia, Turbulent buoyant jets in unstratified surroundings, Int. J. Heat Mass Transfer 19 (1976) 1176–1204.
[26] W. Lin, S.W. Armfield, Very weak fountains in a homogeneous fluids, Numer. Heat Transfer 38 (2000) 377–396.
[27] S. Satyanarayana, Y. Jaluria, A study of laminar buoyant jets discharged at an inclination to the vertical buoyancy force, Int. J. Heat Mass Transfer 25 (1982) 1569–1577.
[28] C. Clannet, On large-amplitude pulsating fountains, J. Fluid Mech. 366 (1998) 333–350.
[29] R.W. Cresswell, R.T. Szczepura, Experimental investigation into a turbulent jet with negative buoyancy, Phys. Fluid 5 (1993) 2865–2878.
[30] S.L. Lee, W.C. Liao, Numerical simulation of a fountain flow on non-staggered Cartesian grid system, Int. J. Heat Mass Transfer 51 (2008) 2433–2443.
[31] L.B. Aldabbagh, I. Sezai, Numerical simulation of three-dimensional laminar, square twin-jet impingement on a flat plate, flow structure, and heat transfer, Numer. Heat Transfer Part A: Appl. 41 (2002) 835–850.
[32] J.Y. San, M.D. Lai, Optimum jet-to-jet spacing of heat transfer for staggered arrays of impinging air jets, Int. J. Heat Mass Transfer 44 (2001) 3997–4007.
[33] S. Popinet, Gerris: a tree-based adaptive solver for the incompressible Euler equations in complex geometries, J. Comput. Phys. 190 (2003) 572–600.